RSC Advances

PAPER

View Article Online
View Journal | View Issue

Cite this: *RSC Adv.*, 2023, **13**, 4746

Graphene oxide as a multi-functional additive for compatilizer, enhancer, and barrier in ethylene vinyl alcohol copolymer/aramid pulp composites

Xuyu Yang, Yingying Ye, Jiayan Liu, Weijun Liu, Xianqiang Xiong and Zhicai He*

To improve the thermal, mechanical, and barrier properties of ethylene vinyl alcohol copolymer (EVOH)/aramid pulp (AP), graphene oxide (GO) was used as a compatilizer, enhancer, and barrier to fabricate EVOH-based composites. The results showed that graphene oxide serves as an ideal compatilizer to reinforce the interfacial action between the EVOH matrix and aramid pulp. The EVOH/AP/GO composite presented the best combination of thermal stability, tensile strength, oxygen barrier, and heat deformation temperature by adding only 1 wt% graphene oxide, compared to those of pure EVOH. Moreover, both scanning electron microscopy (SEM) and polarized optical microscopy (POM) photographs demonstrated that the aramid pulp dispersed homogeneously into the EVOH resin with the addition of 1 wt% graphene oxide. Our work provides a novel and facile way for producing a prominent EVOH-based composite, which can be potentially used in packaging fields in the future.

Received 12th November 2022
Accepted 16th January 2023

DOI: 10.1039/d2ra07182g

rsc.li/rsc-advances

1. Introduction

Packaging films for medicine and food need outstanding gas and moisture barrier performance to ensure the quality of the products during storage and use.[1,2] Ethylene-vinyl alcohol copolymers (EVOH) are widely used in the food packaging industry because of their excellent gas barrier properties, flexibility, and processability.[3,4] The comprehensive performances of EVOH copolymers are dependent on the copolymerization ratio of ethylene to vinyl alcohol. However, the barrier properties, strength, and stiffness of pure EVOH cannot meet the product requirement on certain occasions. To overcome the limited defects and extend its potential applications, the barrier and mechanical properties of EVOH, blending with other polymers, such as nylon 6,[5] poly(vinyl chloride),[6] polystyrene,[7] high-density polyethylene,[8] linear LDPE,[9] polypropylene[10] and poly(methyl methacrylate)[11] for different application have been reported. Besides, the EVOH matrix can also be strengthened with inorganic fillers, such as fiber and graphene, which can decrease the costs of products and improve dramatically the comprehensive properties.[12]

Aramid pulp (AP) is fibrillated by poly-*p*-phenylene terephthalamide (PPTA), known by its trade-name Kevlar, possessing high specific modulus and specific strength, outstanding thermal stability, and lightweight, resulting in a variety of applications in aerospace, military, automotive industry and sports goods.[13,14] Therefore, aramid pulp can be considered an ideal filler to reinforce polyolefin matrix due to its prominent mechanical and thermal properties. Guan *et al.*[15] used aramid nanofibers to reinforce poly(vinyl alcohol) by a solution casting method, and the consequent nanocomposite showed a simultaneously significant enhancement in both strength and toughness. Liu *et al.*[16] incorporated aramid fiber into wood-flour and high-density-polyethylene composites by the extrusion method, and the aramid fiber after modification with dopamine and vinyl triethoxysilane increased the adhesion strength of the resulting composites. However, the surface of AP is composed of ultrafine fibrils, thus, making it difficult to disperse in EVOH because of the inherent inertness and easy entanglement.[17,18] Therefore, the compatibility of EVOH and AP needs to be enhanced so as to maximize the properties of EVOH/AP composites.

Carbon materials have attracted considerable attention since zero-dimension fullerene (C_{60}), one-dimension carbon nanotube (CNT),[19,20] and two-dimension graphene oxide[21] were discovered. In particular, graphene oxide, a flat monolayer of carbon atoms tightly packed into a two-dimensional honeycomb lattice, is considered an excellent additive to reinforce the EVOH matrix because of its gas-impermeable characteristic as well as outstanding mechanical strength and thermal stability.[5] For example, Vuong *et al.*[10] prepared EVOH-based nanocomposites with two graphene and two graphite fillers by melt blending, and the water vapor permeability of the nanocomposite films for 2 wt% fillers decreased by a factor of 1.8 compared to that of pure EVOH. Yang *et al.*[22] prepared high-barrier graphene/EVOH nanocomposites by introducing graphene into the EVOH matrix *via* solution mixing. Their results showed that the permeability coefficient of O_2 for the graphene/EVOH nanocomposite with only 0.5 wt% graphene was

College of Pharmaceutical and Chemical Engineer, Taizhou University, Taizhou, Zhejiang 318000, P. R. China. E-mail: hezhicai@tzc.edu.cn

decreased to 8.517×10^{-15} cm^3 cm cm^{-2} s^{-1} Pa^{-1}, which is nearly 1671 times lower than that of pure EVOH films. However, most of the studies from the literature were only focused on the improvement of the barrier properties by incorporating graphene derives in the polymer matrix,[23] and none have reported the comprehensive improvement of the EVOH composites by using graphene oxide as a compatilizer between organic EVOH and inorganic fibre.

In this study, the homogeneous EVOH/GO masterbatch was prepared using the solvent blending method. Subsequently, the EVOH/AP/EVOH composites with prominent comprehensive properties were fabricated using the melt-blending method, and the new process is suitable for mass production due to the easy operation and low cost. What is more, graphene oxide with oxygen-containing functional groups was used to serve as a compatilizer between EVOH and AP, increasing the interfacial adhesion and optimizing the AP reinforcement. The effect of graphene oxide content on the thermal, mechanical, and barrier properties was investigated, and the morphological structures were characterized using SEM and POM images to explain the interfacial interaction.

2. Experimental

2.1 Materials

EVOH resin with 32% ethylene content was supplied by Kuraray Co., Ltd (Tokyo, Japan). GO was synthesized from purified conventional flake graphite by modified Hummers methods, as reported in our earlier work.[22] Aramid pulps with a length of 0.5–1 mm and bulk density of 48–160 kg m^{-3} were purchased from Dupont.

2.2 Preparation of EVOH/GO masterbatch

The EVOH/GO masterbatch containing 10 wt% graphene oxide was prepared *via* the solvent blending method. Pure EVOH was dissolved in a mixed solvent consisting of water and isopropanol (volume ratio was 1 : 1), and the EVOH solution was kept with magnetic stirring at 90 °C for 120 min. Meanwhile, a given amount of GO was homogeneously dispersed in deionized water using powerful ultrasonic oscillation for 120 min to obtain exfoliated graphene oxide. Then, stable graphene oxide was added into the EVOH mixture at 120 °C for 120 min at the stirring state. These mixtures were dropped onto a cleaned vessel and dried in a vacuum oven at 60 °C until constant weight. Subsequently, these corresponding products were broken to obtain the high concentration of EVOH/GO masterbatch using the plastic cracking machine.

2.3 Preparation of EVOH/AP/GO composites

EVOH/AP/GO composites were fabricated by the melt mixing method. The EVOH/GO masterbatch, pure EVOH, and AP were weighed according to the following formula. In brief, the final weight ratio of EVOH to AP was 90 : 10, and the added amounts of the GO were 0, 0.2, 0.5, 1, and 2 phr. EVOH, AP, and GO were dried at 80 °C for 12 h before the melt mixing.

The dry components were premixed by tumbling and then fed simultaneously into a twin-screw extruder (RC 500P, HAAKE, Germany) to prepare the blends. The extruding temperature for the heating sections was operated between 190 °C to 220 °C, and the screw speed was 100 rpm. The extrudate passed through a cooling water bath and was finally palletized, and then dried in a vacuum oven at 80 °C for 12 h. The dried composite materials were compressed molding with a plate vulcanizing machine at 180 °C for 6 min to obtain a dumbbell-shaped sample for the tensile tests. Film casting of the EVOH/AP/GO composites was performed using a single screw extruder equipped with a 120 mm T-die and a casting roll (Collin cast film line), and the film thickness was controlled to about 20 μm for oxygen by adjusting the speeds of both the extruder screw and the casting roll. For comparison, pure EVOH and EVOH/AP were prepared under the same processing conditions.

For the sake of clarity, the samples were labelled as follows:

EVOH (pure EVOH);

EVOH/AP (EVOH toughened with 10 wt% aramid pulp);

EVOH/AP/0.2%GO (EVOH toughened with 10 wt% aramid pulp and 0.2 wt% graphene oxide);

EVOH/AP/0.5%GO (EVOH toughened with 10 wt% aramid pulp and 0.5 wt% graphene oxide);

EVOH/AP/1%GO (EVOH toughened with 10 wt% aramid pulp and 1 wt% graphene oxide);

EVOH/AP/2%GO (EVOH toughened with 10 wt% aramid pulp and 2 wt% graphene oxide).

2.4 Characterization

Fourier-transform infrared spectroscopy (FTIR) was performed on a PerkinElmer spectrometer using a disc of KBr over the region of 500–4000 cm^{-1}. The morphologies of the fractured surfaces were revealed by scanning electron microscope (SEM, S4800, Japan). The samples were coated with a 10 nm Pt layer. A polarized optical microscope (POM) images of EVOH composites were taken from an optical microscope (Nikon, Japan) equipped with a capture camera. These specimens were heated to 210 °C and melted on glass slides, and then cooled to room temperature to obtain the microscopic images. Thermogravimetry analysis (TGA) was performed on a PerkinElmer thermal analyzer under the N_2 atmosphere at a heating rate of 10 °C min^{-1}. The nominal melting temperature of the samples was measured using the differential scanning calorimeter (DSC-Q10) in the temperature range from 30 °C to 250 °C at 10 °C min^{-1}; the temperature was kept at 250 °C for 2 min and then decreased at a linear rate of 10 °C min^{-1} from 250 to 30 °C, and the heating–cooling cycle was recorded again. Tensile tests were performed on a universal tension test machine (CMT-4104, SANS Group, China) at a strain rate of 10 mm min^{-1} until the fracture occurred according to the ASTM D-412 standard. Dynamic mechanical analysis (DMA) was performed using a DMA Q800 (TA instruments Inc., USA) from 30 to 150 °C at a constant rate of 2 °C min^{-1}.

The heat deformation temperature (HDT) of the EVOH composite was further investigated by using a heat deformation

Vicat temperature testing machine (HV-3000, Institute of Intelligence testing machine, Changchun, China). Samples were heated from room temperature at a linear heating rate of 2 °C min^{-1} on the basis of the CNS 11643 standard. Oxygen transmission rates (OTRs) of the EVOH/AP/GO composite films were measured with an oxygen permeability testing machine (Jinan Languang Mechanical and Electrical Technology Co, Ltd, China). OTR tests were carried out at 23 °C and 37% relative humidity according to the Chinese standard method of GB 1038-2000.

3. Results and discussion

Fig. 1 illustrates the schematic reaction of graphene oxide with EVOH and AP. There are several intermolecular hydrogen bonds between EVOH and GO because of the abundant oxygen-containing groups at the surface of GO,[22] and the dehydration reaction might occur between the amido groups of aramid pulp and the carboxyl groups of GO.[24,25]

FTIR spectra were recorded to determine the chemical structure; as shown in Fig. 2, the typical peaks of GO appear at 3439, 1632, and 1066 cm^{-1}, corresponding to the presence of hydroxyl, carboxyl and epoxy groups, respectively. Compared to the –OH bond stretching peak (3468 cm^{-1}) of EVOH, those of EVOH/AP and EVOH/AP/1%GO are shifted to a lower wavenumber (3452 cm^{-1} and 3442 cm^{-1}, respectively) with the decrease of peak height and the increase of peak width, suggesting the formation of hydrogen bond that arose between EVOH and graphene oxide.[26] Besides, the absorption peaks at

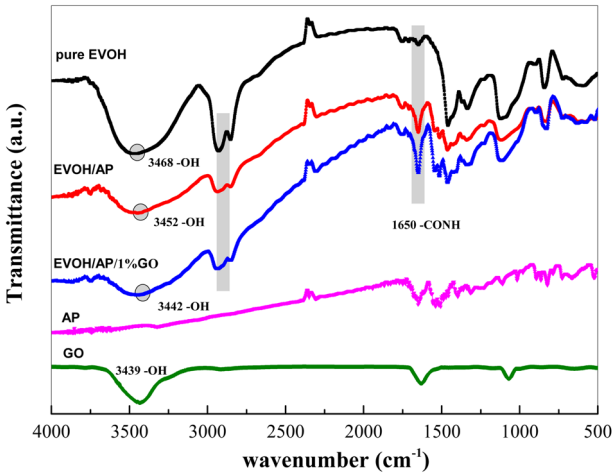

Fig. 2 FTIR spectra of pure EVOH and EVOH/AP/GO composites.

2920 and 2850 cm^{-1} of EVOH composite corresponding to the C–H stretching vibrations of $-CH_2$ and –CH groups became weak due to the introduction of aramid pulp and graphene oxide. Moreover, the increasing intensity of the absorption peak at 1650 cm^{-1} is assigned to the formation of the amide bonds, implying the chemical combination in the compound interface.[27] All the results confirm the strong interactions of hydrogen bonding and amide group between the EVOH matrix and aramid pulp.

To investigate the morphological structures and interfacial interaction, SEM images of impact fracture samples were

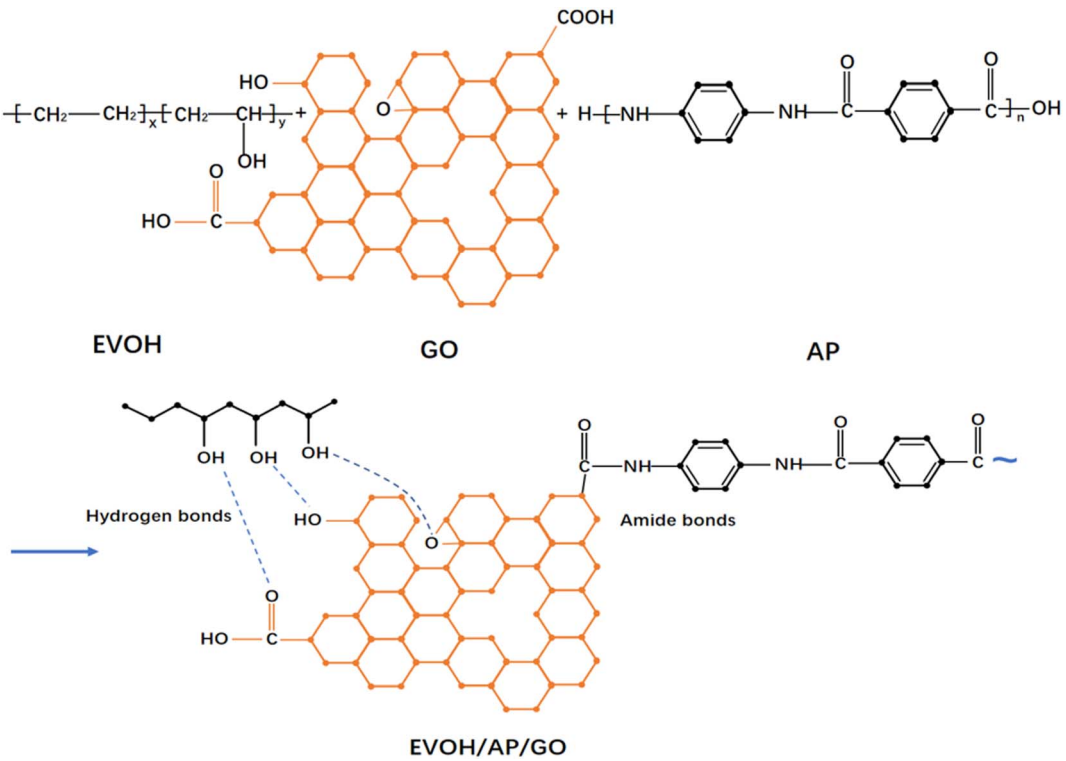

Fig. 1 Reaction schematic of graphene oxide with EVOH and AP.

collected and are displayed in Fig. 3. The fracture surface of pure EVOH is smooth and fluctuates like a mountain range (Fig. 3a). After the introduction of 10% aramid pulp into EVOH, a large number of AP agglomerations are exposed to the surface of the resin (Fig. 3b), implying the poor compatibility between inorganic AP and organic EVOH. These agglomerations in composites may cause stress concentration points and prevent the load from transferring to the EVOH matrix.[28] In contrast with the EVOH/AP composite, the aramid pulp into the composite became shorter and dispersed homogeneously with the increasing content of graphene oxide (from Fig. 3c, b to Fig. 3e). However, a few agglomerations, including shorter aramid pulp at the surfaces of the composite can be easily observed for the composite containing 2 wt% graphene oxide (Fig. 3f), and the poor dispersion may originate from the aggregation of excessive graphene oxide through π–π stacking and van der Waals interactions.

POM was also used to characterize the crystallization morphology and interfacial action of pure EVOH and EVOH/AP/GO composites. POM micrographs are shown in Fig. 4 with a large vision scope, implying the important influence of graphene oxide on pure EVOH and EVOH/AP/GO composites. As can be seen from Fig. 4a, pure EVOH displays common α-spherulites with a large number of little spherulites. With the incorporation of 10 wt% aramid pulp, long fibers with large size disperse inhomogeneously in the EVOH matrix (illustrated in Fig. 4b). As shown in Fig. 4c and d, the average size of aramid pulp was decreased prominently and no visible aggregations were observed due to the addition of graphene oxide, which is assigned to the combination of the strong chemical and hydrogen bonding. However, extensive agglomerations can be easily observed on the surfaces of the composites containing 2 wt% graphene oxide (Fig. 4e), and the poor dispersion might

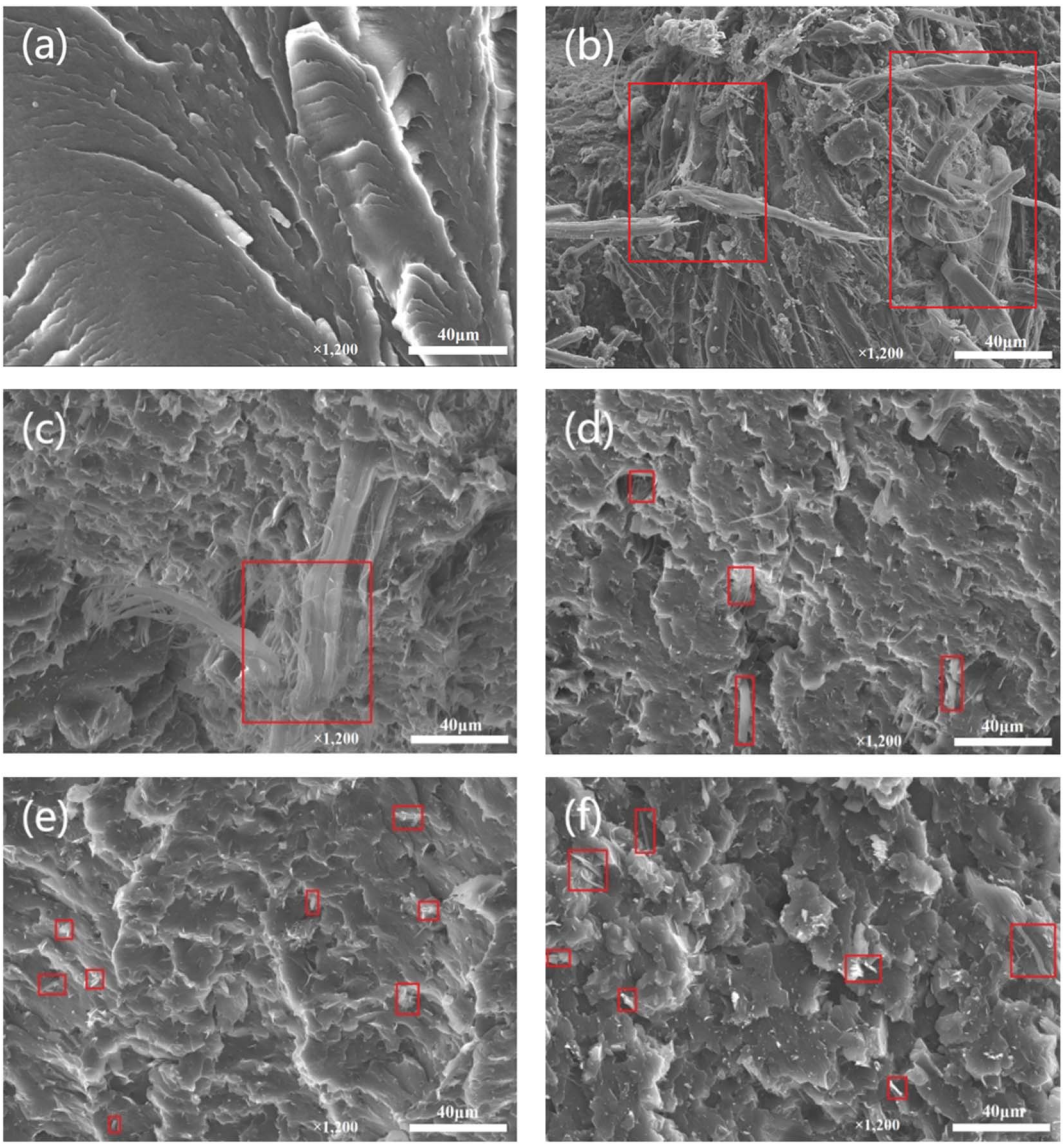

Fig. 3 SEM images of the fracture surface of (a) EVOH, (b) EVOH/AP, (c) EVOH/AP/0.2% GO, (d) EVOH/AP/0.5% GO, (e) EVOH/AP/1% GO, (f) EVOH/AP/2% (red rectangles represent aramid pulp).

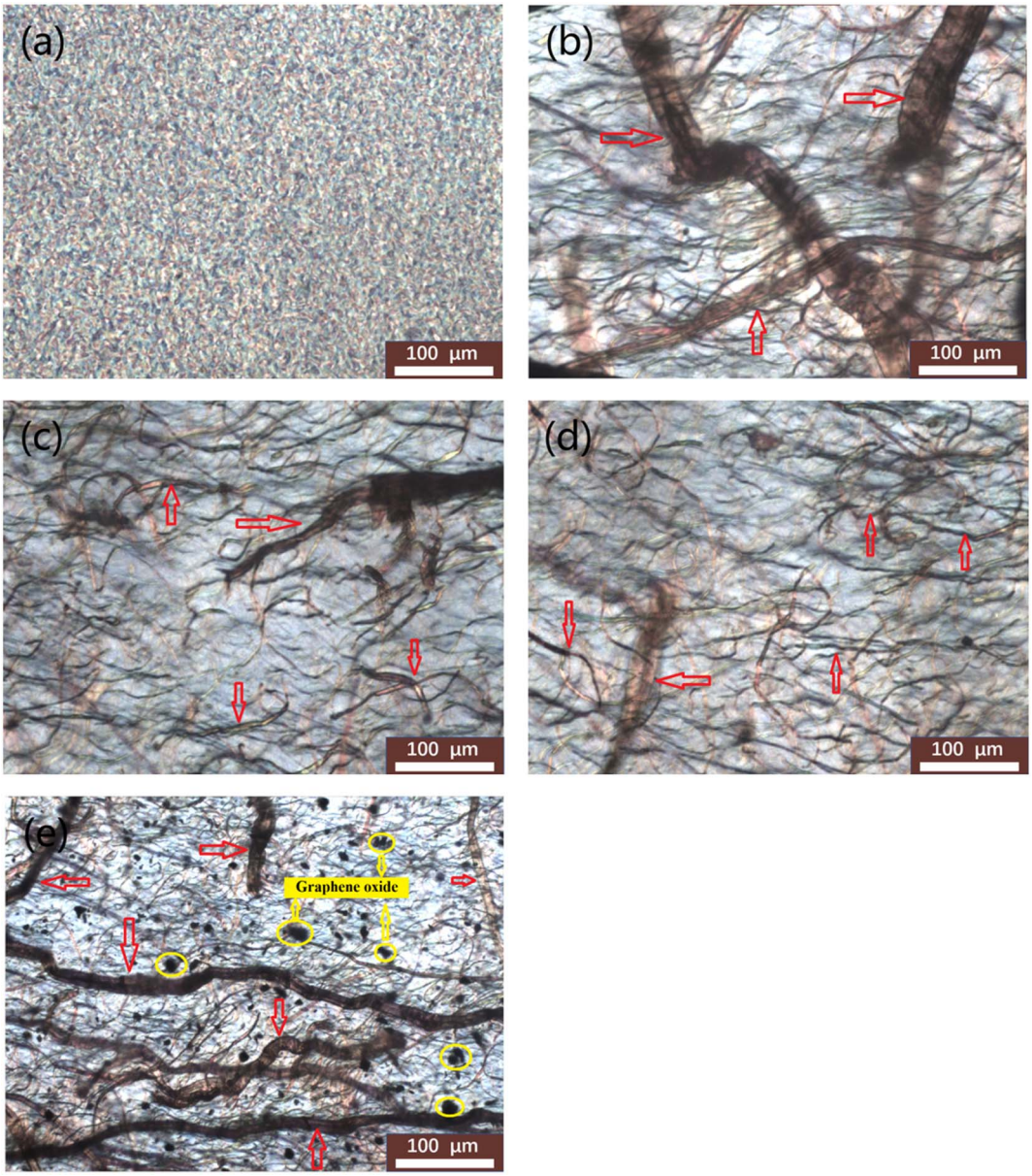

Fig. 4 POM micrographs of (a) EVOH, (b) EVOH/AP, (c) EVOH/AP/0.2% GO, (d) EVOH/AP/0.5% GO, (e) EVOH/AP/2% GO (×200) (red arrows point to aramid pulp and yellow circles represent graphene oxide).

be attributed to the agglomerations of excessive graphene oxide.[29]

TGA and DSC experiments were performed to investigate how graphene oxide content affects the thermal stability of EVOH composites. Fig. 5a shows the thermogravimetric curves (TG) of pure EVOH and the EVOH/AP composites with different mass fractions of GO under a nitrogen atmosphere. According to the inserted table of the derivative thermogravimetric curves shown in Fig. 5b, the maximum decomposition temperatures (T_{max}) of the EVOH/AP composite are improved with the increasing contents of graphene oxide. The maximum decomposition temperature of EVOH/AP occurs at about 419.3 °C, while that of EVOH/AP after incorporation of 0.2, 0.5, 1, 2 wt% GO are increased by 4 °C (423.3 °C), 11.8 °C (431.1 °C), 17.7 °C (437.0 °C) and 16.3 °C (435.6 °C), respectively. The thermal stability of the EVOH composites is prominently improved by the addition of graphene oxide, which can be attributed to the homogeneous distribution of the aramid pulp into the EVOH matrix by using GO as a compatilizer. Besides, the unique two-dimensional structure of graphene oxide may be serving as a barrier to heat transfer and prevent the emissions of small gaseous molecules.[30]

The melting temperature (T_m) of these samples was measured using DSC on the second scan. As listed in Fig. 5c, the T_m value (177.6 °C) of the EVOH/AP composite is comparatively higher than that of EVOH (172.5 °C), implying that the aramid pulp might serve as reinforced material to restrict the chain mobility of the EVOH matrix. Furthermore, the melting temperatures of the EVOH/AP composites are improved with the increasing addition (under 1 wt%) of graphene oxide, while

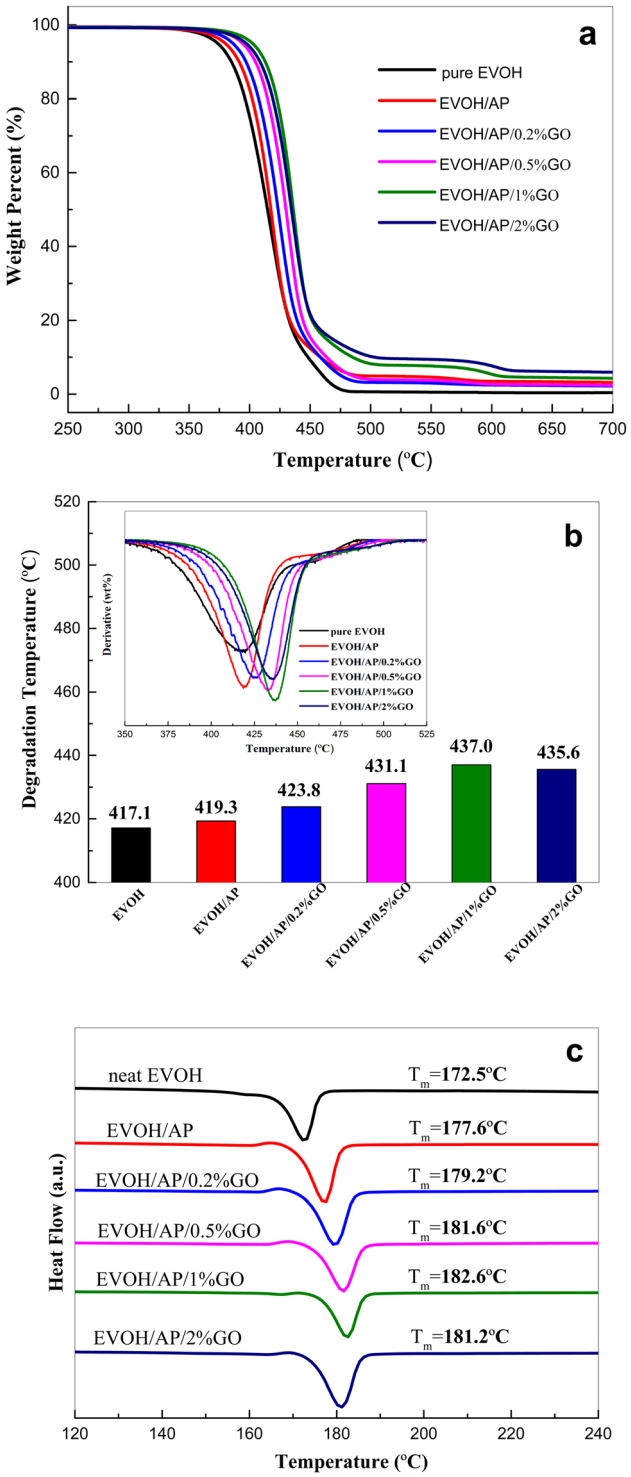

Fig. 5 Typical (a) TG, (b) maximum degradation temperature, and (c) non-isothermal curves of pure EVOH and EVOH/AP/GO composites with various graphene oxide loadings. T_m: melting temperature. The insets in (b) exhibit DTG curves of pure EVOH and EVOH/AP/GO composites.

that of the EVOH/AP/GO composites, including 2 wt% graphene oxide tend to decline due to the poor dispersion of EVOH and the fillers.

To evaluate the mechanical reinforcing effect from the incorporation of GO into the EVOH resin, typical stress–strain curves of pure EVOH and EVOH/AP/GO composites with various amounts of GO were collected as shown in Fig. 6. Compared to pure EVOH, EVOH/AP counterparts containing 10 wt% AP exhibit higher tensile strength and Young's modulus, but the elongation at the break of EVOH/AP decreased dramatically, which can be related to poor interaction between AP and EVOH. The loading contents of GO in the EVOH matrix have an important influence on the mechanical properties of the composites. With the increase of GO content (less than 1 wt%), both the tensile strength and Young's modulus of EVOH/AP/GO composites rise sharply, while the elongation at the break increases first and decreases afterwards in comparison with EVOH/AP. The incorporation of 1 wt% graphene oxide causes a substantial increase in the tensile strength, Young's modulus, and the elongation at the break of the composite by approximately 57%, 28%, and 400%, respectively, compared with those of the EVOH/AP composite. Such an enhancement of the mechanical properties can be ascribed to the unique two-dimensional structure of graphene oxide. Besides, graphene oxide acts as a compatibilizer and promotes the homogeneous dispersion of AP between the two phases, which improves the interfacial interaction and thus promotes a better stress transfer between the AP and EVOH matrix. However, as seen from the SEM results, both the tensile strength and the elongation at the break are negatively affected when the contents of graphene oxide are up to 2 wt%. The results may be attributed to the agglomeration of excessive graphene oxide due to the existence of the van der Waals force, which makes the interaction weak and caused defeats between the AP and EVOH matrix.

Dynamic mechanical thermal analysis (DMTA) curves of the EVOH/AP/GO composites are presented in Fig. 7. As shown in Fig. 7a and b, the values of loss tangent ($\tan\delta$) and storage modulus (E') for EVOH/AP/GO composites tend to increase with the increasing content of GO. Glass transition temperature (T_g) of pure EVOH, and EVOH/AP, EVOH/AP/0.2% GO, EVOH/AP/

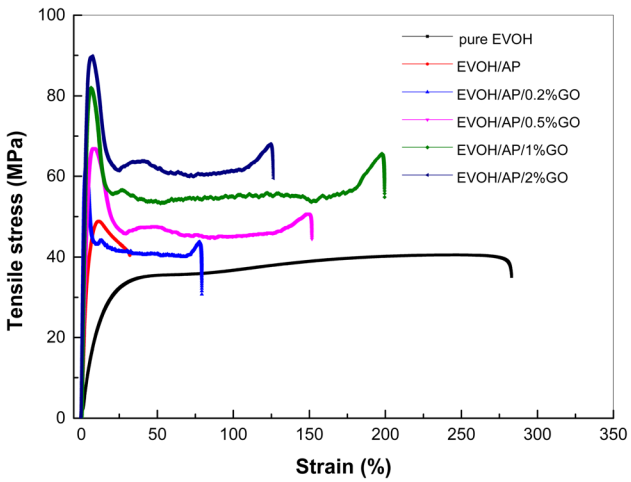

Fig. 6 Typical stress–strain curves of pure EVOH and EVOH/AP/GO composites.

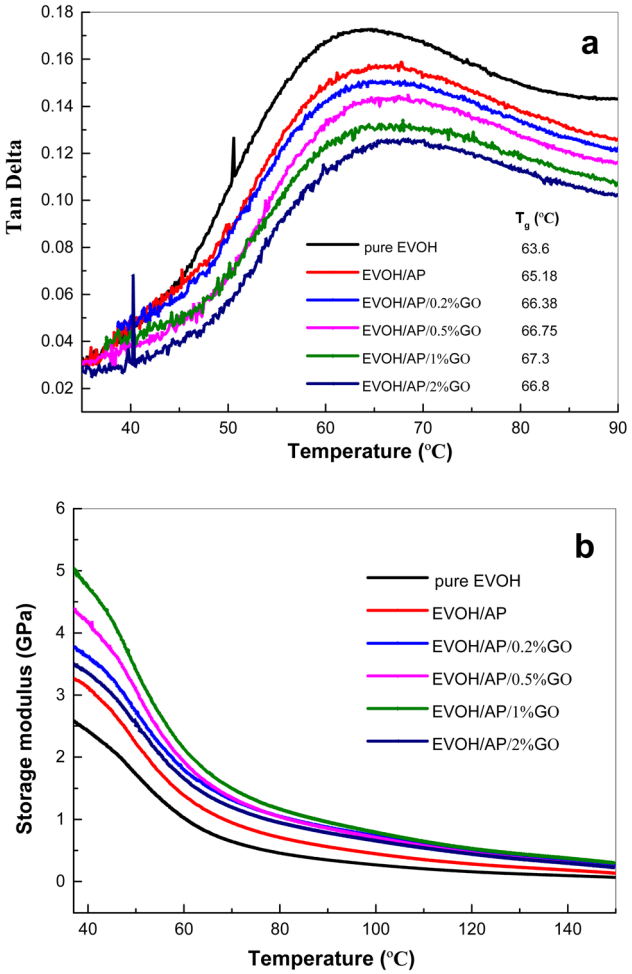

Fig. 7 Curves of (a) loss tan δ and (b) storage modulus *versus* temperature for pure EVOH and EVOH/AP/GO composites.

0.5% GO, EVOH/AP/1% GO and EVOH/AP/2% GO are 63.6, 65.18, 66.38, 66.75, 67.3 and 67.8 °C, respectively. An addition of 10%wt of the aramid pulp could increase the storage modulus of the EVOH matrix due to the rigidity of AP, restricting the molecular movement of the composites and causing the improvement of the glass transition temperature. With the increasing addition of graphene oxide, the T_g and E' values increase simultaneously, which are ascribed to the strong interfacial interactions between the aramid pulp and the EVOH matrix because graphene oxide acts as a compatilizer, inhibiting the mobility of the EVOH chains. In particular, graphene oxide may serve as a fiber-reinforced material and improve the mechanical properties of the EVOH matrix.

HDT testing results of EVOH and EVOH/AP/GO composites are presented in Fig. 8. HDT of pure EVOH occurs at about 73.8 °C, which is significantly inferior to the heat-resistant temperature of plastic products used in our daily life. The HDT values of EVOH composite are increased to 106.8 °C by the incorporation of 10 wt% aramid pulp. Compared with that of EVOH/AP, the HDT values of EVOH/AP/GO composites with the addition of 0.2, 0.5, 1, 2 wt% are increased by 12.6 °C (119.4 °C), 20.9 °C (128.7 °C), 26.9 °C (133.7 °C), and 21.3 °C (128.1 °C),

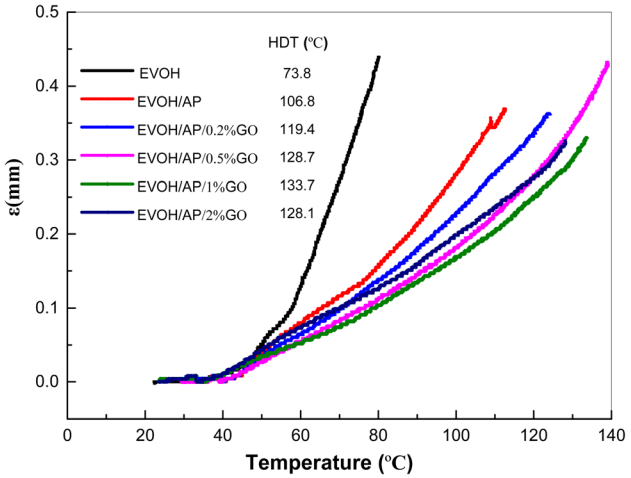

Fig. 8 HDT curves of pure EVOH and EVOH/AP/GO composites.

respectively. HDT properties of the EVOH/AP/GO composites are significantly enhanced by the addition of graphene oxide, which might be attributed to the homogeneous distribution of the aramid pulp into the EVOH matrix and the high aspect ratio of graphene oxide.[31]

Graphene oxide is considered an efficient barrier to prevent gas molecules, such as oxygen and water vapor because of its unique two-dimensional structure and high aspect ratio.[32] Permeability coefficients of pure EVOH and EVOH/AP/GO composites are shown in Fig. 9. The pure EVOH and EVOH/AP have oxygen permeability coefficients of 56.79 and 107.72 $\times$ 10^{-15} cm^3 cm cm^{-2} s^{-1} Pa^{-1}, respectively. With the incorporation of 0.2, 0.5, 1 and 2 wt% graphene oxide, the oxygen permeability coefficients of EVOH/AP/GO were prominently improved to 21.64 $\times$ 10^{-15}, 10.63 $\times$ 10^{-15}, 4.83 $\times$ 10^{-15}, and 2.77 $\times$ 10^{-15} cm^3 cm cm^{-2} s^{-1} Pa^{-1}, respectively. The remarkable improvement in the oxygen barrier performance was observed by the incorporation of only a small content of

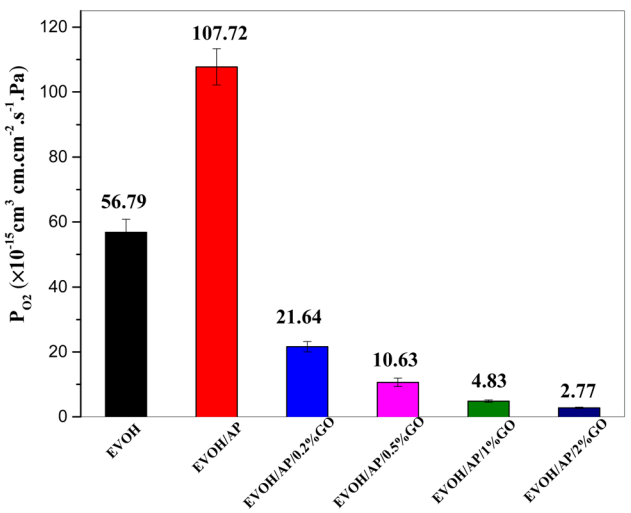

Fig. 9 Permeability coefficients (P_{O_2}) of pure EVOH and EVOH/AP/GO composites.

graphene oxide, increasing the tortuous path for penetrating gases.[33,34]

4. Conclusion

The EVOH/AP/GO composites with improved thermal stability, and mechanical and barrier properties were fabricated successfully. FTIR studies demonstrated that graphene oxide served as a compatilizer to improve the interfacial interaction by chemical combinations. From both SEM and POM observations, the aramid pulp displayed a tiny size and diffused uniformly into the EVOH composite with the addition of 1 wt% graphene oxide, but a few agglomerations at the surfaces of the composite can be easily observed with excessive graphene oxide (2 wt%), comparing these results with these of pure EVOH, the comprehensive performances of EVOH/AP/GO composites increased firstly and fell subsequently with the increased incorporation of graphene oxide. It is emphasized that the incorporation of graphene oxide at only 1 wt% into the EVOH matrix promoted the interfacial interactions between aramid pulp and EVOH resin, resulting in a substantial enhancement in thermal and mechanical properties, heat deformation temperature, and oxygen transmission rates. In our work, graphene oxide was used as compatilizer, enhancer, and barrier in EVOH/aramid pulp composites, which provides an effective means to improve the comprehensive properties as packaging materials for various applications.

Conflicts of interest

There are no conflicts to declare.

Acknowledgements

The work has been supported by Zhejiang Provincial Natural Science Foundation (GG21E03008 and LQ21B030003), Taizhou Science and Technology Project (No. 21gya28). China.

References

1 S. E. Chavez, H. Ding, B. L. Williams, S. Nam, Z. Hou, D. Zhang and L. Sun, *ES Mater. Manuf.*, 2021, **15**, 72–77.
2 A. M. LaChance, Z. Hou, M. M. Farooqui, S. A. Carr, J. M. Serrano, C. E. Odendahl, M. E. Hurley, T. E. Hurley, T. E. Morrison, J. L. Kubachka, N. T. Samuels, A. T. Barrett, Y. Zhao, A. M. DeGennaro, M. H. Camara and L. Sun, *Adv. Compos. Hybrid Mater.*, 2022, **5**, 1–11.
3 A. Blanchard, F. Gouanvé and E. Espuche, *Polymers*, 2021, **13**, 3546.
4 D. Xu, X. Zheng and R. Xiao, *RSC Adv.*, 2017, **7**, 7108–7115.
5 W. Lu, C. Lu, J. Hu, J. Wu and Q. Zhou, *Polym. Eng. Sci.*, 2021, **61**, 1719–1731.
6 A. Tarasov, D. Rauhut and R. Jung, *Food Chem.*, 2018, **268**, 463–467.
7 Y. Jin, Q. Zhu, W. Zhong, K. Yan and D. Wang, *J. Phys. Chem. C*, 2018, **123**, 185–194.
8 M. Sun, S. Zhu, C. Zhang, A. Olah, E. Baer and D. A. Schiraldi, *ACS Appl. Polym. Mater.*, 2019, **1**, 259–266.
9 J. Feng, Z. Li, A. Olah and E. Baer, *J. Appl. Polym. Sci.*, 2018, **135**, 46425.
10 S. Vuong, L. Léger and F. Restagno, *Polym. Eng. Sci.*, 2020, **60**, 1420–1429.
11 J. A. de Lima and M. I. Felisberti, *Eur. Poylm. J.*, 2008, **44**, 1140–1148.
12 J. Kim, S. Oh, S. M. Cho, J. Jun and S. Kwak, *J. Appl. Polym. Sci.*, 2020, **137**, 49537.
13 E. F. Kerche, V. D. da. Silva, E. Fonseca, N. A. Salles, H. S. Schrekker and S. C. Amico, *Polymers*, 2021, **226**, 123787.
14 H. Jiang, F. Cheng, Y. Hu, Y. Ji, X. Hu and Y. Ren, *Compos. Sci. Technol.*, 2021, **206**, 108664.
15 Y. Guan, W. Li, Y. Zhang, Z. Shi, J. Tan, F. Wang and Y. Wang, *Compos. Sci. Technol.*, 2017, **144**, 193–201.
16 W. Liu, Y. Li, S. Yi, L. Wang, H. Wang and J. Zhang, *Polymers*, 2021, **13**, 236.
17 G. Jiang, L. Yu, M. Zhang and F. Wang, *Polym. Adv. Technol.*, 2020, **31**, 853–863.
18 R. Vallabh, A. Li, P. D. Bradford and D. Kin, *J. Text. Inst.*, 2022, **113**, 1799–1805.
19 Y. Zhang, L. Liu, L. Zhao, C. Hou, M. Huang, H. Algadi, D. Li, Q. Xia, J. Wang, Z. Zhou, X. Han, Y. Long, Y. Li, Z. Zhang and Y. Liu, *Adv. Compos. Hybrid Mater.*, 2022, **5**, 2601–2610.
20 P. Wang, T. Song, H. M. Abo-Dief, J. Song, A. K. Alanazi, B. Fan, M. Huang, Z. Lin, A. A. Altalhi, S. Gao, L. Yang, J. Liu, S. Feng and T. Cao, *Adv. Compos. Hybrid Mater.*, 2022, **5**, 1100–1110.
21 W. Yu, S. Li, H. Yang and J. Luo, *RSC Adv.*, 2020, **10**, 15328–15345.
22 J. Yang, L. Bai, G. Feng, X. Yang and M. Lv, *Ind. Eng. Chem. Res.*, 2013, **52**, 16745–16754.
23 Y. Cui, S. Kumar, B. R. Kona and V. H. Daniel, *RSC Adv.*, 2015, **5**, 63669–63690.
24 L. Zhang, S. Zhou, L. Xie, L. Wen, J. Tang, K. Liang, X. Kong, J. Zeng, R. Zhang, J. Liu and B. Kong, *Small*, 2021, **17**, 2100141.
25 J. Ji, Q. Kang, Y. Zhou, Y. Feng, X. Chen, J. Yuan, W. Guo, Y. Wei and L. Jiang, *Adv. Funct. Mater.*, 2017, **27**, 1603623.
26 L. Zhang and L. Liu, *Nanoscale*, 2019, **11**, 3656–3664.
27 E. Valeur and M. Bradley, *Chem. Soc. Rev.*, 2009, **38**, 606–631.
28 S. Han, Q. Meng, X. Pan, T. Liu and S. Zhang, *J. Appl. Polym. Sci.*, 2019, **136**, 48056.
29 H. Tang, Y. Zhao, S. Shan, X. Yang, D. Liu, F. Cui and B. Xing, *Environ. Sci.: Nano*, 2018, **5**, 2357–2367.
30 P. C. Okonkwo, W. Emori, P. C. Uzoma, I. B. Mansir, A. B. Radwan, O. O. lge and A. M. Abdulah, *Int. J Energy Res.*, 2022, **46**, 3766–3781.
31 Y. Gao, O. T. Picot, E. Bilotti and T. Peijs, *Eur. Poylm. J.*, 2017, **86**, 117–131.
32 S. W. Kim and H. M. Choi, *High Perform. Polym.*, 2015, **27**, 694–704.
33 Y. Cui, S. I. Kundalwal and S. Kumar, *Carbon*, 2016, **98**, 313–333.
34 D. Dutta, A. N. F. Ganda, J. K. Chih, C. C. Huang, C. J. Tseng and C. Y. Su, *Nanoscale*, 2018, **10**, 12612–12624.